ELSEVIER

Polymer 40 (1999) 5833–5842

polymer

Calorimetric and dielectric study of a blend containing a conductive polymer: poly(3-octylthiophene) + poly(ethylene-co-vinylacetate)

Miguel A. Monedero[a], Gustavo S. Luengo[a], Susana Moreno[a], Francisco Ortega[a], Ramón G. Rubio[a,*], Margarita G. Prolongo[b], Rosa M. Masegosa[c]

[a]*Department of Química- Física I, Facultad Química, Universidad Complutense, 28040 Madrid, Spain*
[b]*Department of Materiales y Producción Aerospacial, ETSI Aeronáuticos, Universidad Politécnica, 28040 Madrid, Spain*
[c]*Department of Tecnologías Especiales Aplicadas a la Aeronáutica, E.U.I.T. Aeronáuticos, Universidad Politécnica, 28040 Madrid, Spain*

Received 24 August 1998; received in revised form 29 October 1998; accepted 29 October 1998

Abstract

The phase diagram of the binary system poly(3-octylthiophene) + poly(ethylene-co-vinylacetate), P3OT + EVA was studied by Differential Scanning Calorimetry (DSC). The blends of low and high content of P3OT were found to be homogeneous. The system was also studied by a dielectric relaxation technique in the frequency range 20 Hz–100 kHz. The complex electric modulus M^* is discussed in terms of the well-known Havriliak–Negami function. We also obtained the spectrum of relaxation times using a regularization technique. The spectra allowed us to calculate the d.c. conductivity. A low frequency contribution to the dielectric loss found in two-phase samples was attributed to interface polarisation effects. © 1999 Elsevier Science Ltd. All rights reserved.

Keywords: Differential scanning calorimetry; Dielectric relaxation; Conductivity

1. Introduction

Conducting polymers have attracted much attention during the last few years because of potential technological applications [1]. From the academic point of view, they are examples of disordered electronic conductors [2]. Even though there exists a reasonably good level of understanding about the conducting mechanisms in these materials [3], the use of conducting polymers in technological applications has been somehow precluded by their poor processability and high cost.

Blending conducting polymers may help overcome both problems. Most of the blends containing a conducting polymer have been found to be immiscible [4–6]. As far as conductivity is concerned, this is not a problem, as immiscibility can lead to multipercolation processes, thereby lowering the percolation threshold [7]. From the mechanical point of view, good adhesion between coexisting phases is necessary, which is favoured when the composition of each phase is not too close to the pure components [8]. In recent years, binary blends showing a miscibility window have been reported [9,10].

Ngai and Rendell [11] showed that conducting polymers present strong conductivity relaxations over relatively broad frequency ranges. This has been confirmed later by other authors [12], who also used the Kohlraush–Williams–Watts (KWW) relaxation curve in order to describe the complex permittivity (electrical modulus) in the range 1 Hz–1 MHz, and over broad temperature ranges. In general, a good description of the experimental data is obtained, and the results clearly indicate that the frequently used Jonscher equation [13] for describing the conductivity in nonconducting polymers is not valid for conducting ones.

In the case of blends some further complications may be expected. On one side, blending polymers usually tends to broaden the relaxations, therefore making the description of their relaxation processes in terms of a single KWW curve, more complicated [14]. However, in the case of immiscible blends, the existence of interfaces between the two coexisting phases may give rise to interface polarization effects [15], thus adding further structure to the relaxation spectra of the systems.

Several conducting blends have been studied in the microwave region (20 MHz–20 GHz), as reflection and transmission S_{ij}-parameters in this region are necessary to characterise the materials for electronic-shielding and radar absorption applications [16,17]. However, not much has been done in the 10 Hz–1 MHz region where the interference between conduction, electrode polarisation, and structural relaxations may be the largest.

* Corresponding author.

0032-3861/99/$ - see front matter
PII: S0032-3861(98)00810-6

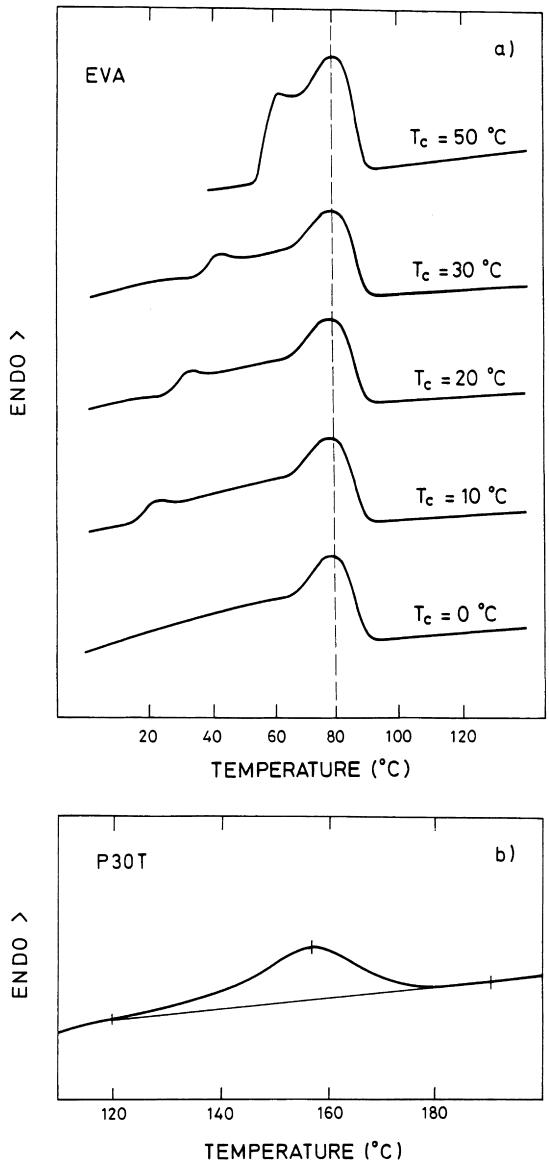

Fig. 1. (a) Endotherms of EVA in the melting region. Notice that while the high temperature peak is almost insensitive to the crystallization temperature T_c, the low temperature one tends to merge with the first one with increasing T_c. (b) Endotherm for pure P3OT.

We have chosen the system poly(3-octylthiophene) (P3OT) + poly(ethylene-co-vinylacetate) with 20% vinylacetate units, (EVA). P3OT is a soluble conducting polymer, and has been extensively studied by Chen et al. [12,18] at frequencies below 1 MHz. The frequency dependence of the electrical modulus of P3OT is rather well described in terms of the KWW relaxation function. EVA has also been studied by several authors [19,20], the copolymer shows a rather low dielectric activity (max. $\epsilon''(\omega) < 0.1$), which frequency dependence is well described by the Havriliak–Negami (H–N) function.

Levon et al. [9] have described the EVA-rich region of the phase diagram of the P3OT + EVA, and found a noticeable region of miscibility for temperatures below the melting point of P3OT. Moreover, they found that in the mid-composition range, despite of the system being thermodynamically unstable, phase separation is precluded below the melting point of EVA because of the existence of EVA crystallites.

As already mentioned, the P3OT + EVA system has been studied, for a limited composition range, in the microwave region [17], however, there are no detailed dielectric studies at lower frequencies. The aims of the present work are to carry out such a study, and to compare the most frequently used method for describing conductivity relaxation (i.e. describing M^* in the frequency domain by means of the KWW or the H–N functions), with a method based on the calculation of the relaxation spectra from the frequency dependence of the real and the imaginary components of M^*[21].

The rest of the article is organised as follows: Section 2 gives some details of the experimental methods. Section 3 discusses the results and their implications. Finally Section 4 summarises the main conclusions.

2. Experimental section

Both P3OT and EVA were obtained from POLYSCIENCES (Germany). EVA was used as received, while P3OT was dissolved in chloroform, filtered and reprecipitated with benzene. This step was necessary as some insoluble particles were found in the original sample. Gel Permeation Chromatography (GPC) from tetrahydrofuran solutions gave the following values for M_n, and polydispersity index: (2500, 2.6) for P3OT and (85 000, 2.4) for EVA. ^{1}HNMR spectra for EVA confirm that the content of vinyl acetate in EVA was very close to 20%.

The blends were prepared by casting from solutions of the appropriate amounts of each polymer in chloroform. The solvent was eliminated in a vacuum oven, keeping the temperature at least 20°C below the melting point of EVA. The samples for dielectric measurements were moulded under pressure at 50°C.

The glass transition temperatures, (T_gs), and melting points were measured with a PERKIN ELMER DSC-4 calorimeter. A standard 20°C /min heating rate was used. Sample weights ranging from 10 to 15 mg were used, and the measurements were carried out under dry N_2 atmosphere. The glass transition temperatures were taken at the midpoint of the heat capacity transition. The melting point temperatures, T_m, of each endotherm were located at the maxima of their respective peaks.

The following heat treatment was followed in the DSC for the melting point measurements: the samples were kept at 200°C for a period of 10 min to ensure the complete melting of the components. Then they were rapidly cooled to the crystallisation temperature (T_c), and kept at T_c for a period of 20 min, before being cooled to −10°C. The melting behaviour was monitored by heating at 20°C/min.

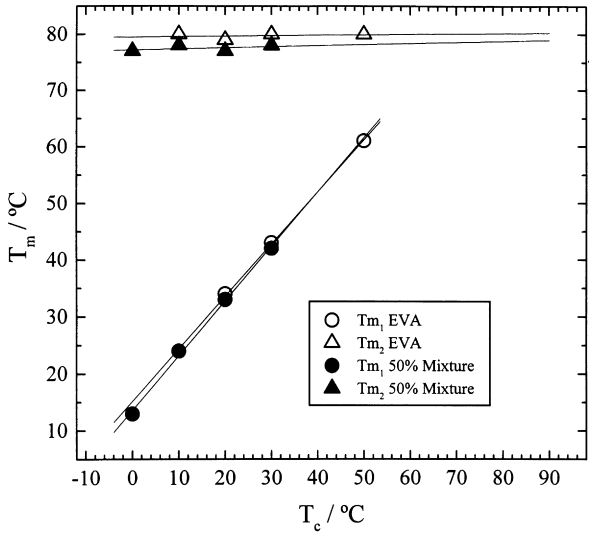

Fig. 2. Temperatures corresponding to the two melting peaks of EVA as a function of T_c for pure EVA and for a blend with 50% of P3OT.

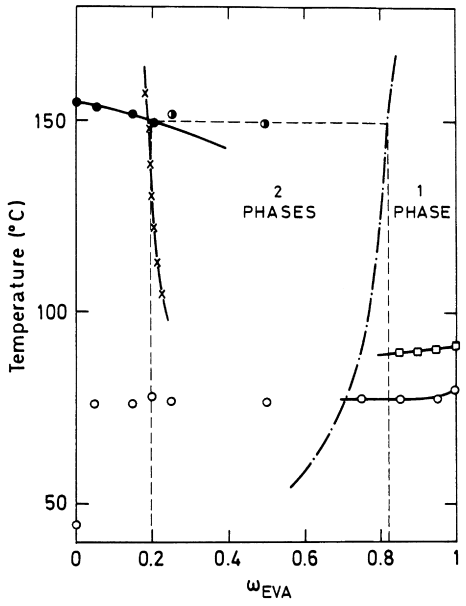

Fig. 3. Phase diagram of the EVA + P3OT system. (o), melting points of the P3OT in the P3OT-rich phase. (◇) and (□), melting points of the EVA from this work and from Ref. [9], respectively. (○) melting points of immiscible blends. The dash-dotted line is the binodal curve reported in Ref. [9] by visual observation.

A POLYMER SCIENCE (UK) DETA system was used for the dielectric relaxation experiments in the 20 Hz–100 kHz frequency range, using a parallel plate capacitor. Circular samples, 33 mm in diameter and 0.2 mm thick were used. In order to check whether the interface electrode-sample had a significant effect in the measurements, the results using raw and silver-plated samples were compared.

3. Results

3.1. Calorimetry

We have obtained the T_g values -26°C for EVA and -9°C for P3OT, which are in good agreement with the values reported in the literature [12,19]. The broad glass transitions and the proximity of the T_gs do not allow discussion of the miscibility of the system in terms of the existence of one or two T_gs. However, the melting point may be a useful tool. While P3OT gives a relatively weak melting point, EVA leads to two peaks, one strongly dependent on the crystallisation temperature, T_c while the other is nearly independent of T_c. A similar situation was found for the blends. Fig. 1 shows the thermograms for the pure polymers. Fig. 2 summarises the results of the melting temperatures from the two endotherms of EVA as a function of the crystallisation temperature for pure EVA and for the blend with 50% P3OT.

The increase of T_m with T_c is a consequence of the more perfect crystals grown at lower supercooling. The Hoffman–Weeks equation:

$$T_m^0 - T_m = \phi(T_m^0 - T_c) \quad (1)$$

describes the melting of isothermally crystallized samples, T_m^0 being the equilibrium melting temperature, and ϕ the stability parameter, which depends on the thickness of the crystal. $\phi = 0$ corresponds to the most stable crystals, and $\phi = 1$ to the less stable ones. The melting endotherms at lower temperatures correspond to ϕ values close to 0.92, thus indicating low stability of the structures formed. Moreover, the melting temperature of these samples is relatively independent of the blend composition. However, values of ϕ close to 0.01 were obtained for the high temperature melting process, which indicates that the crystals formed are fairly stable. These endotherms show a noticeable melting depression with the increase of P3OT content. This is in accordance with Levon's results [9], and suggests the miscibility of blends rich in EVA.

Our results for T_m can be combined with the data of Levon et al. [9] to complete the phase diagram shown in Fig. 3. It points out that for $w_{P3OT} \geq 0.75$ there is a decrease in the melting point of P3OT that also suggests miscibility in this composition range. Unfortunately, in this composition range the melting point of EVA is affected by a relatively large uncertainty, and ranges between 76°C and 78°C. It should be noted that while P3OT crystallises from a melt, EVA does it from a matrix containing P3OT crystallites. However, for $0.5 \leq w_{P3OT} \leq 0.75$ the T_m of P3OT takes values higher than those expected from a simple extrapolation of the melting point line for $w_{P3OT} \leq 0.25$, thus suggesting phase separation. For $w_{P3OT} \leq 0.4$ the trace of melting of P3OT is too weak to be detected.

A plot of T_m^{-1} vs. $(1 - \phi_2)^2$ (ϕ_2 being the volume fraction of P3OT) leads to straight lines, as predicted by the Nishy–Wang equation for blends that form miscible amorphous phases [22]. It has not been possible to calculate the

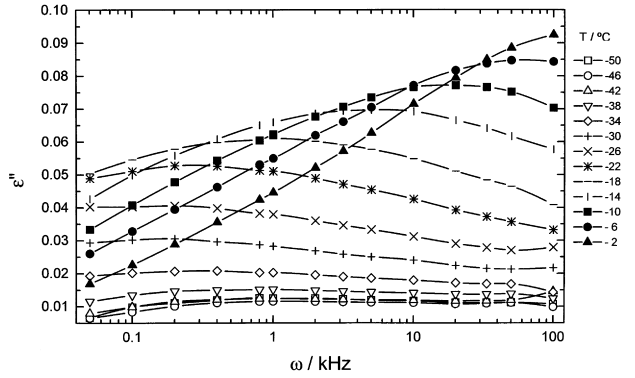

Fig. 4. Imaginary component of the dielectric permittivity of pure EVA as a function of temperature and frequency.

polymer–polymer interaction parameter because of the lack of the enthalpy of fusion of pure P3OT. However, the slope of the Nishy–Wang equation for EVA is several times lower than that for P3OT, thus suggesting that the enthalpy of fusion for pure P3OT is also much lower than that of EVA.

3.2. Dielectric relaxation

3.2.1. Pure polymers

As already mentioned, the dielectric responses of EVA and P3OT are rather different. Fig. 4 shows the imaginary component of ϵ^* for EVA. The $\epsilon''(\omega)$ vs. ω curves follow the time-Temperature Superposition Principle (tTSP) for a reduced frequency range of 10^{-3}–10^{3} kHz. As shown by Buerger and Boyd [19], and by Hozer and Strobl [20], $\varepsilon^*(\omega)$ can be well described by the H–N equation [22]

$$\frac{\epsilon^*(\omega) - \epsilon_u}{\Delta\epsilon} = \left[1 + (i\omega\tau_{HN})^{1-\alpha}\right]^{-\gamma}, \tag{2}$$

$$\Delta\epsilon = \epsilon_r - \epsilon_u \qquad 0 \le (1-\alpha), \quad \gamma \le 1, \tag{3}$$

where ϵ_r refers to the zero frequency permittivity, and ϵ_u to its infinite frequency limit. α, γ and τ_{HN} are adjustable parameters, that may depend on T. α takes care of the symmetric broadening of the $\epsilon''(\omega)$ vs. lg ω curves while γ allows Eq. (2) to describe asymmetric broadening [22]. Under certain restrictive conditions for the α and γ parameters, the H–N function leads to equivalent results compared to the KWW relaxation function [23]. The results obtained in this work for $\epsilon''\omega$ and $\epsilon'\omega$ can be well described by setting $\gamma = 1$, as can be observed in Fig. 5. The temperature dependence of α and $\Delta\epsilon$, ϵ_r and ϵ_u can be well described by a straight line for the temperature range studied. Table 1 shows the results of the fits of each of the above parameters to straight lines. The present values are in good agreement with those of Refs. [19,20]. From the frequency of the maximum of the $\epsilon''(\omega)$ vs. lg ω curves ω_m, we have calculated the relaxation time

$$\tau_m = (2\pi\omega_m)^{-1}. \tag{4}$$

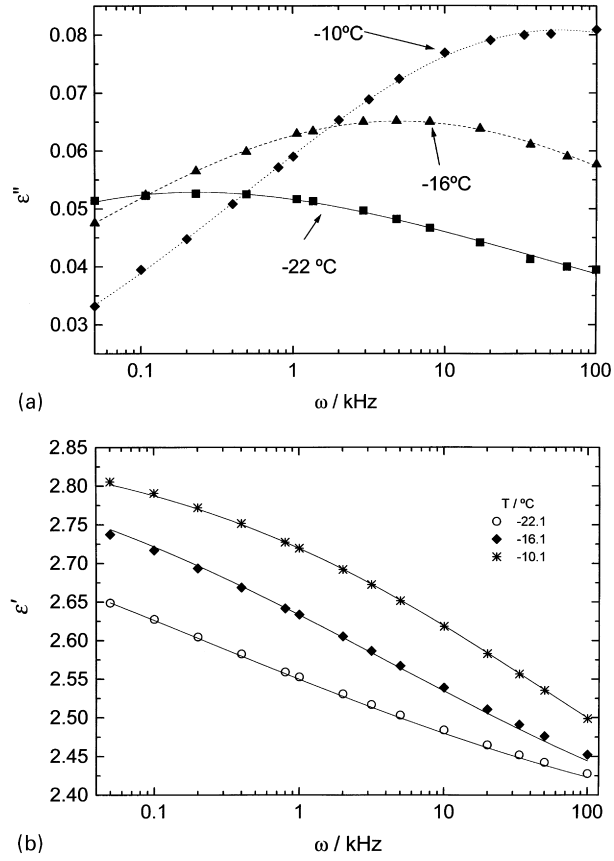

Fig. 5. Comparison of the experimental data of ϵ'' (a) and ϵ' (b) for EVA at three temperatures, with the predictions of the Havriliak–Negami equation using the parameters of Table 1.

The temperature dependence of τ_m has been fitted to the Williams–Landel–Ferry equation [24]

$$\log a_T = lg\frac{\tau_m}{\tau_0} = -\frac{C_1(T - T_0)}{C_2 + T - T_0}, \tag{5}$$

where a_T is called the shift factor, C_1 and C_2 are adjustable parameters, characteristic of each system, and τ_0 is the relaxation time at a reference temperature T_0. Fig. 6 shows the shift factor, and Table 2 collects the constants of Eq. (5).

As the $\epsilon''(\omega)$ vs. lg ω do not show maxima within our frequency range for P3OT, the data are better discussed in terms of the electrical modulus $M^* = 1/\epsilon^*$. Fig. 7 shows the experimental data for M'', as well as the master curve. It also shows that the KWW relaxation function gives a good description of the master curve, except for the high frequency range. The value of the parameter β, characteristic of the KWW function takes values $0.62 \le \beta \le 0.64$ between -28°C and -4°C, very close to the values reported by Chen and Liao [12] for the same temperature range.

As will be shown later, the KWW function does not correlate correctly the $M''(\omega)$ vs. lg ω curves for the blends, hence we have described $M''(\omega)$ using

$$M''(\omega) = \frac{\epsilon''(\omega)}{\epsilon'^2(\omega) + \epsilon''^2(\omega)} \tag{6}$$

Table 1
Characteristic parameters of the different fits of ϵ_u, γ, α and $\Delta\epsilon$

w_{P3OT}	$\epsilon_u = \epsilon_{u0} + \epsilon_{u1}\cdot T$		$\gamma = \gamma_o + \gamma_1$ T (K)		$\alpha = \alpha_o + \alpha_1\cdot T$		$\Delta\epsilon = \Delta\epsilon_o + \Delta\epsilon_1\cdot T + \Delta\epsilon_2\cdot T^2 + \Delta\epsilon_3\cdot T^3$			
	ε_{u_0}	ε_{u_1} K^{-1}	γ_o	$\gamma_1 \times 10^3$ K^{-1}	α_o	$\alpha_1 \times 10^3$ K^{-1}	$\Delta\epsilon_o$	$\Delta\epsilon_1$ K^{-1}	$\Delta\epsilon_2$ K^{-2}	$\Delta\epsilon_3$ K^{-3}
0.0	4.15	−0.0074	1.0 ± 0.0	0.0 ± 0.0	2.5 ± 0.2	6.7 ± 0.7	−0.5 ± 0.5	(4.0 ± 2.0) 10^{-3}	0	0
0.10	3.21	−0.0030	1.5 ± 0.3	−2.0 ± 1.0	2.3 ± 0.2	6.0 ± 0.6	(6.0 ± 1.5) 10^{3}	−54 ± 14	(1.5 ± 0.4) 10	(1.5 ± 0.5) 10^{-4}
0.20	2.42	−0.0026	0.3 ± 0.3	2.0 ± 1.0	0.6 ± 0.2	0.7 ± 0.6	(1.5 ± 0.4) 10^{3}	−14 ± 4	(0.5 ± 0.1) 10	(5.0 ± 2.0) 10^{-5}
0.30	0.31	0.0054	0.8 ± 0.3	0.3 ± 1.0	0.3 ± 0.2	0.0 ± 0.6	−2.5 ± 0.7	(2.3 ± 0.2) 10^{-2}	0	0
0.50	1.02	0.0032	−0.1 ± 0.2	3.7 ± 0.8	−0.3 ± 0.1	2.2 ± 0.4	0.7 ± 0.7	(1.2 ± 0.2) 10^{-2}	0	0
0.70	1.46	0.0019	−0.5 ± 0.2	4.9 ± 0.8	−0.5 ± 0.1	2.5 ± 0.4	6.3 ± 0.7	(1.1 ± 0.2) 10^{-2}	0	0
1.0	2.88	−0.0019	0.48 ± 0.05	0.7 ± 0.2	0.0 ± 0.0	0.0 ± 0.0	9.6 ± 1.0	(2.2 ± 0.4) 10^{-2}	0	0

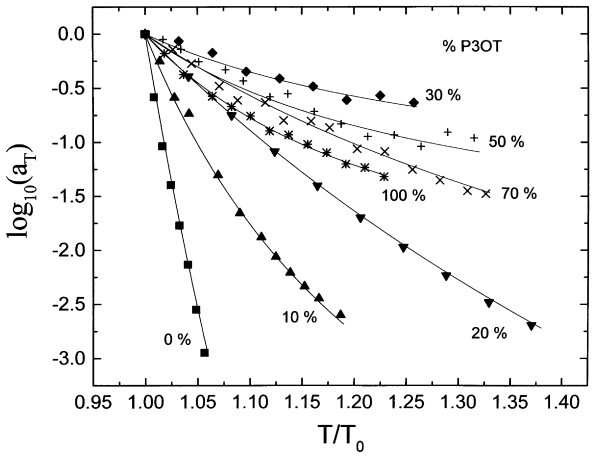

Fig. 6. Shift factors for the EVA + P3OT blend through the whole composition range of weight fractions w_{P3OT}. The lines represent the fits to the WLF equation with the parameters of Table 2.

with ϵ' and ϵ'' given by Eq. (2). Fig. 8 shows the results for three of the isotherms. The quality of the fits is similar to the one obtained with the KWW relaxation function. As can be observed, in the high frequency range the H–N function underestimates the experimental data. Table 1 collects the fits of the H–N parameters for the temperature range studied in this work. It is worth noting that contrary to the results for EVA, for P3OT, $\alpha = 0$, and $\gamma \ni 1$. Fig. 6 shows that the temperature dependence of the shift factor is much smaller than for pure EVA. The present results allow the calculation of the zero-frequency limit of the conductivity $\sigma_{d.c.}$

$$\sigma_{d.c.} = \frac{\epsilon_0}{M_u \langle \tau_p \rangle}, \tag{7}$$

where ϵ_0 is the vacuum permittivity, $M_u = /\epsilon_u$, and $\langle \tau_p \rangle$ is the mean relaxation time. The calculation of $\sigma_{d.c.}$ from the H–N function was done through the following steps. From Eq. (2) we have calculated the relaxation spectrum $H_{N-N}(\tau)$ using the parameters of Table 1, and then the relaxation curve $\phi(t)$ [21]. Finally $\langle \tau_p \rangle$ was obtained as

$$\langle \tau_p \rangle \int_{0>}^{\int} \phi(t)\, dt. \tag{8}$$

Although for P3OT the $\phi(t)$s were well described by a KWW function, this will not be in the case of blends, were

Table 2
WLF parameters for the EVA + P3OT system at different compositions

w_{P3OT}	τ_0/s	C_1	C_2 K^{-1}	T_0 K
0.0	0.17690	17 ± 7.0	72 ± 33	249 ± 0.2
0.10	9.30000	6.4 ± 0.6	76 ± 11	289 ± 0.2
0.20	3.94000	10 ± 0.2	255 ± 7	243 ± 0.1
0.30	0.02570	1.6 ± 0.5	89 ± 47	250 ± 2.0
0.50	0.02492	2.1 ± 0.4	71 ± 24	237 ± 1.0
0.70	0.02316	4.7 ± 1.0	164 ± 53	226 ± 1.0
1.0	0.10795	2.8 ± 0.2	57 ± 6	218 ± 0.4

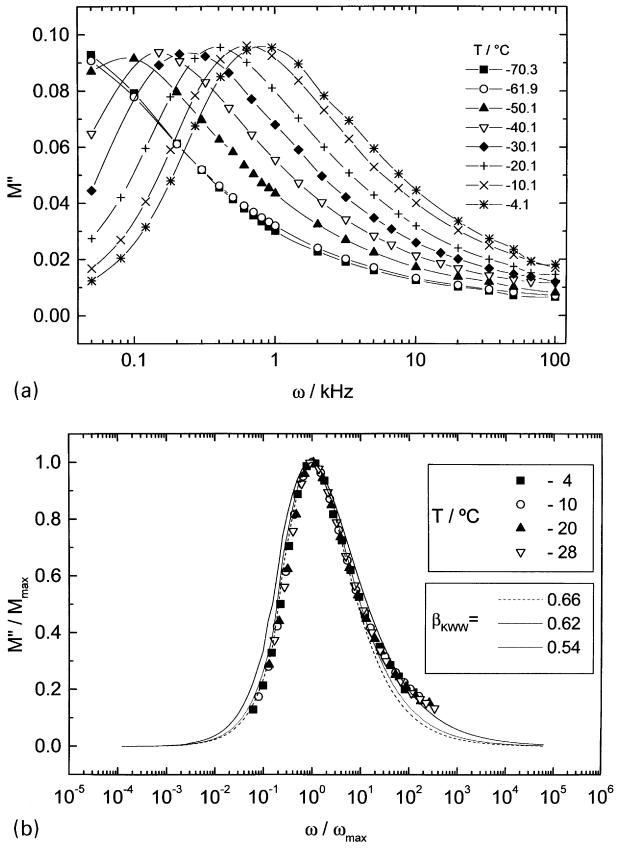

Fig. 7. (a) Experimental results of the imaginary component of the electrical modulus $M''(\omega)$ for pure P3OT. (b) Master curve of M'' for pure P3OT. The curves represent predictions of the KWW function for the values of the stretching parameter β shown.

significant differences were found in the long time (i.e. low ω) region. Fig. 9 shows the values of $\sigma_{\text{d.c.}}$ obtained by the method just described. As it can be observed, the agreement with the values reported by Chen and Liao [12] is satisfactory, through all of our temperature range, which means that, for this polymer, the KWW and the H–N fits are equivalent.

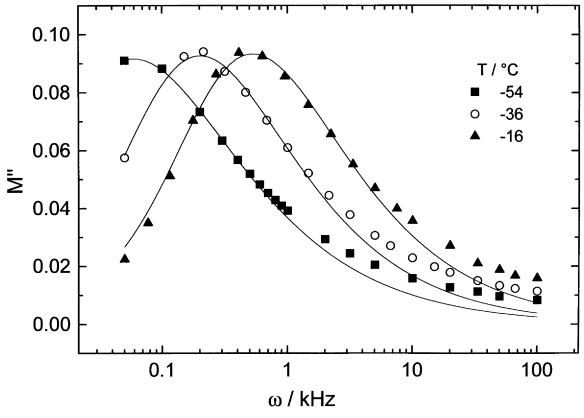

Fig. 8. Best fits for the imaginary component of the electrical modulus of pure P3OT from the H–N equation at three temperatures. The parameters used are given in Table 1.

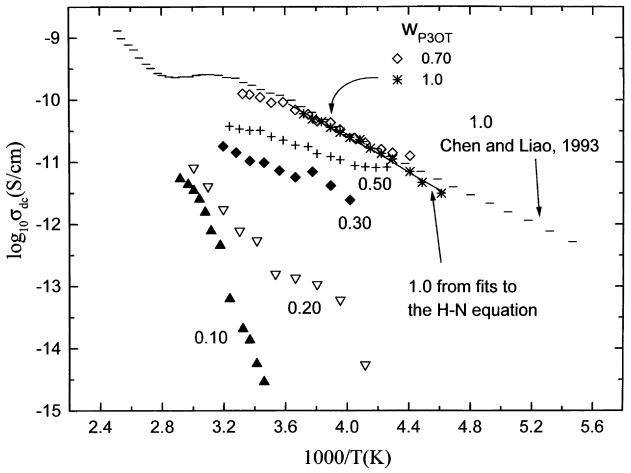

Fig. 9. Conductivity (d.c.) for the EVA + P3OT blend over the whole composition range. The composition is expressed in weight fraction of P3OT, w_{P3OT}. The results of Ref. [12] for pure P3OT are included for the sake of comparison. Symbols represent the values obtained from the relaxation spectra. The continuous curve represents the values obtained for P3OT from the fits to the H–N equation.

3.2.2. Blends

In the case of blends containing less than 30% of P3OT, $\epsilon''(\omega)$ continuously decreases with increasing ω, while for blends richer in P3OT, $\epsilon''(\omega)$ presents maxima at frequencies below 1 kHz. Fig. 10 shows the results for the blends at 10°C. For the sake of uniformity we will discuss the results in terms of M^*.

Fig. 11 shows M'' for five different blends, with weight fraction of P3OT ranging from 0.1 to 0.7, and for temperatures well below the melting temperature of EVA. The first aspect to mention is that the curves are broader than for pure P3OT. We have tried to describe the $M''(\omega)$ vs. lg ω curves using a KWW function, however the results have been quite unsatisfactory as neither the width nor the asymmetry of the curves can be described. It was even impossible to follow Moynihan's suggestion [25], of fitting the data for $10^{-2} \leq \omega(\tau) \leq 10^{2}$, as the KWW function either the high

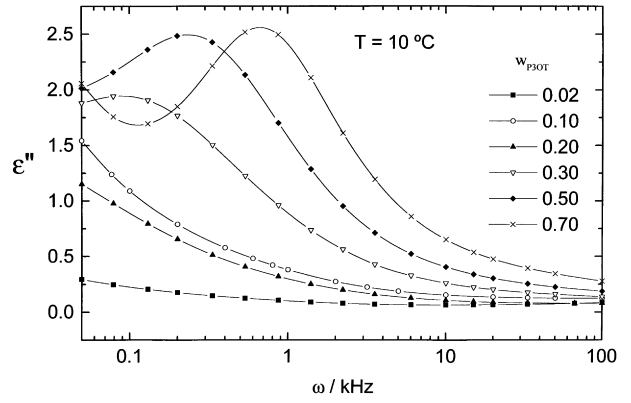

Fig. 10. Imaginary component of the dielectric permittivity of the EVA + P3OT blend at 10°C and for different blend compositions. The curves are aid for the eyes.

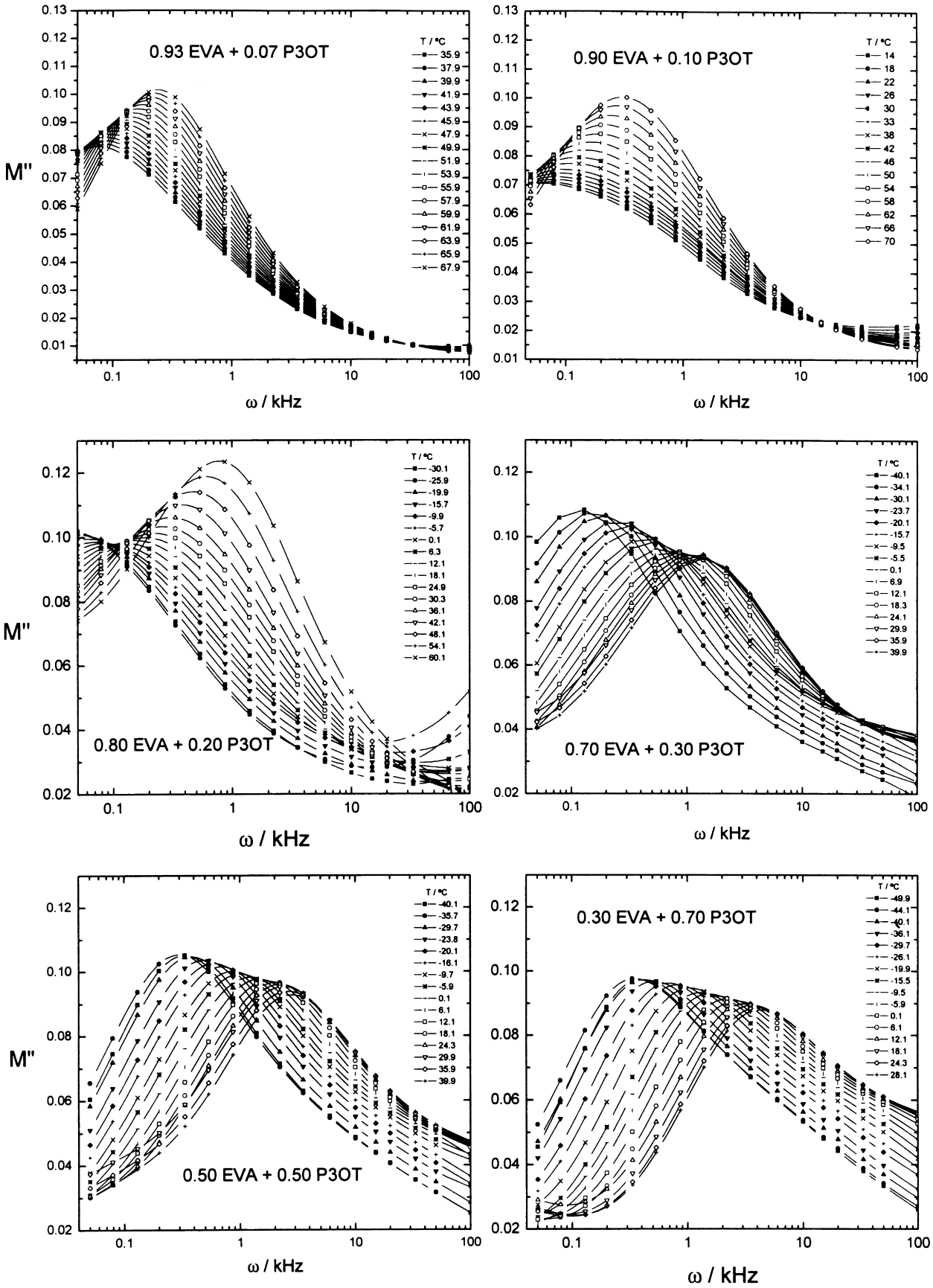

Fig. 11. Imaginary component of the electric modulus M^* for different compositions and temperatures for the EVA + P3OT blends.

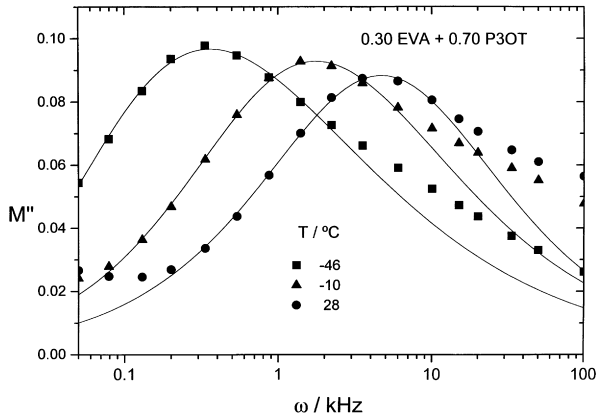

Fig. 12. Comparison of the experimental values of M'' and the best fits of the H–N equation for the blend with $w_{P3OT} = 0.70$. The parameters used are given in Table 1. Similar results were obtained for other compositions.

frequency or the low frequency sides of the curve were not accounted for. This is not a completely surprising result, as one may expect that in this blend concentration fluctuations will play a significant role, thus broadening the relaxation curves. Roland and Ngai [26] have suggested the use of distribution of KWW functions for dealing with this kind of situation. In a previous work [27] we have found that this may lead to good correlation of the data, but it is always at the expense of introducing further adjustable parameters, which affects the calculation of $\sigma_{d.c.}$ and are difficult to control.

The H–N function does a better job than a single KWW, however, as can be observed in Fig. 12 for one of the blends, only the central part of the relaxation curves is described. Table 1 gives the constants that describe the linear fits of the parameters of the H–N equation, and the constants of the WLF equation.

Following the work on pure conducting polymers, one might be tempted to assign the central peak of the $M''(\omega)$ vs. lg ω curves to the conductivity relaxation [11,12]. As already seen, this leads to satisfactory results for pure P3OT, where the H–N function leads to a good fit of the data. However, this is a less safe method for the blends, and hence an alternate procedure, based on the calculation of the relaxation spectrum H(τ) from the experimental $M''(\omega)$ and $M'(\omega)$ data, was followed and is described later.

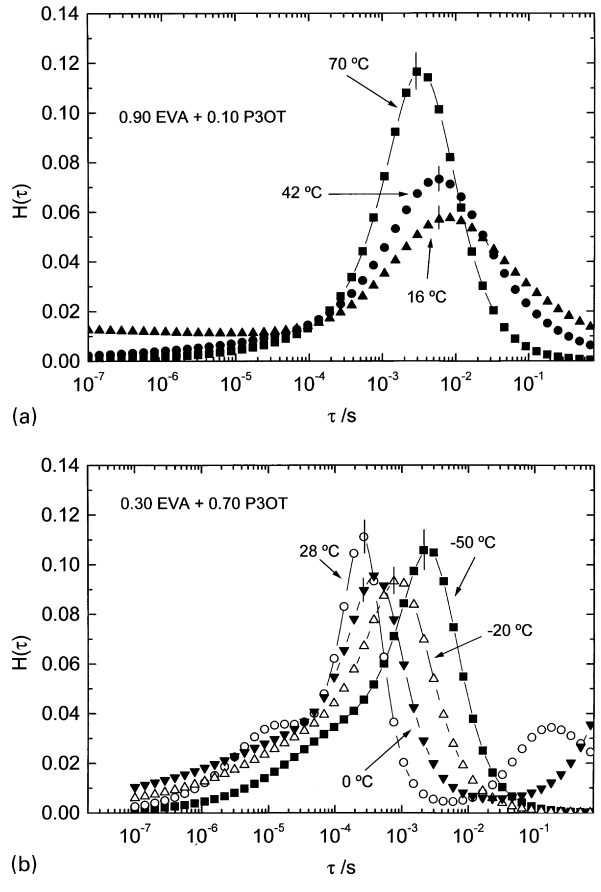

Fig. 13. Temperature dependence of the relaxation spectra for two blends with $w_{P3OT} = 0.10$ (homogeneous sample) (a) and $w_{P3OT} = 0.70$ (nonhomogeneous sample) (b).

3.2.3. Relaxation spectra

The real and imaginary parts of $M^*(\omega)$ can be related to the spectrum of relaxation times by [28]

$$\frac{M'(\omega) - M_r}{\Delta M} = \int_{-\infty}^{\infty} H(\ln\tau) \frac{\omega^2\tau^2}{1 + \omega^2\tau^2} \mathrm{d}\ln\tau, \tag{9a}$$

$$\frac{M''(\omega)}{\Delta M} = \int_{-\infty}^{\infty} H(\ln\tau) \frac{\omega\tau}{1 + \omega^2\tau^2} \mathrm{d}\ln\tau, \tag{9b}$$

where $M_r = 1/\varepsilon_r$, and $\Delta M = M_u - M_r$. Calculating $H(\tau)$ from noisy experimental data over a limited frequency range can be done using constrained regularisation methods [29]. In the present work we have made use of the method proposed by Weese et al. [30] to describe simultaneously $M'(\omega)$ and $M''(\omega)$ within their experimental uncertainties. The algorithm also provides the value of M_r. A similar method based on the CONTIN algorithm has been used recently by Alvarez et al. [31], and Rizos et al. [32]. When used for analysing dynamic light-scattering data, both algorithms lead to indistinguishable results.

Fig. 13 shows the relaxation spectra for two of the blends at different temperatures. It can be observed that for the blend with 10% of P3OT, which is in the one-phase region of the phase diagram shows only one well-defined peak. However, for blends rich in P3OT more complex shapes appear with a well-defined peak at low frequency (long relaxation times), which intensity increases with T. A small high-frequency shoulder appears at the highest temperatures. These effects become more evident in Fig. 14, where the effect of composition at constant $|T - T_g|$ is shown.

Once the components of the relaxation spectrum and M_r are available, the calculation of $\langle\tau_p\rangle$ and of $\sigma_{d.c.}$ is straightforward. The results are shown in Fig. 9. The first point to

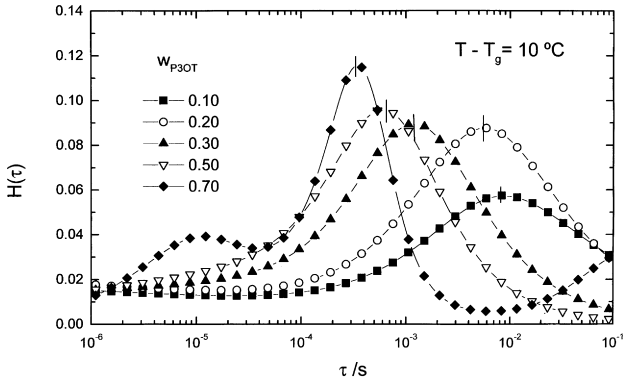

Fig. 14. Composition dependence of the relaxation spectra of the EVA + P3OT blend for a constant value $|T - T_g| = 10°$.

remark is that the results obtained for pure P3OT are coincident with those obtained from the fits to the H–N function and again they are in good agreement with the results of Chen and Liao [12] obtained from fits to the KWW function.

In the case of blends rich in P3OT we have assigned the main peak of H(τ) to the conductivity of the sample, as it can be continuously followed from blends with 10% of P3OT to the ones with high content of conducting polymer. The peak that appears at high values of τ was assigned to the interfacial polarisation effects that may be expected in inhomogeneous systems. Although the low frequency limit of our experiments is too high to explore in detail the polarisation contributions, the raw experimental data, represented as complex admittance is consistent with the present interpretation. The small shoulder at low values of τ may be because of structural (dipolar) relaxation. Fig. 9 shows the values of $\sigma_{d.c.}$ for the P3OT + EVA blend. As can be observed, the effect of T is much higher for the homogeneous blends ($w_{P3OT} < 0.30$) than for the inhomogeneous ones. We have calculated the shift factor a_T from $\langle\tau_p\rangle$, and the results are shown in Fig. 6. The values obtained for pure P3OT from fits to the H–N equation and from the present method are coincident within their uncertainties. Fig. 6 also shows the fits to the WLF equation. The comparison of Figs. 6 and 9 suggests that, for the temperature range studied, there is a close qualitative correlation between the d.c. conductivity and the fragility of the samples. It must also be remarked that the difference in conductivity among the different samples tends to decrease as the temperature is raised.

The relaxation spectrum allows estimation of the different contributions in the dielectric permittivity. This may be better done for samples rich in P3OT, where a maximum is observed in the $\epsilon''(\omega)$ vs. ω curves. As an example, Fig. 15 shows the three contributions for the blend with 70% of P3OT at 227 K. As can be observed, the structural contribution is rather small over the whole frequency range, in agreement with the conclusions of Ngai and Rendell [11]. The conductive contribution accounts for most of the dielectric dispersion above 1 kHz. However, in the low frequency

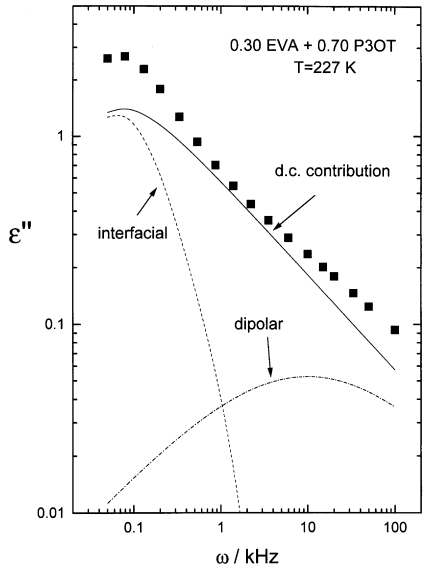

Fig. 15. Conductivity, interfacial and dipolar contributions to the imaginary component of the dielectric permitivity for the blend with $w_{P3OT} = 0.70$. Comparable results have been obtained for other nonhomogeneous samples.

range the interfacial polarisation contribution accounts for half the value of ϵ'' at $\omega \approx 100$ Hz. These interfacial effects are known to be very important in inhomogeneous systems [15,33]. Fitting $M''(\omega)$ vs. log ω to models such as the H–N or the KWW functions, may allow the separation of conductive, structural and interfacial contributions if broad-band dielectric data are available. Otherwise, the parameter characteristic of each of the contributions is highly correlated, and the separation may be difficult [34]. Although, of course, the use of regularization methods to analyse the M' and M'' data does not add any new physical information, we have found that the method is rather robust, and gives consistent estimations of $\sigma_{d.c.}$ even if the experimental data cover a limited frequency range.

4. Conclusions

The DSC analysis of the melting points of the P3OT + EVA blend has allowed us to complete the phase diagram of the system. At low temperature the blend is homogeneous for weight fractions of P3OT $w_{P3OT} < 0.3$ and $w_{P3OT} > 0.7$. The complex electric modulus data were analysed in terms of the Havriliak–Negami function. An algorithm based on regularization methods was used to obtain the spectrum of relaxation times. From the spectrum we have calculated the d.c. conductivity, and the contributions from interfacial polarisation processes and from structural relaxation. It was found that for two-phase samples, the conductive contribution accounts for most of the dielectric loss above 1 kHz, and that the interfacial contribution is very significant below that frequency. The effect of temperature on $\sigma_{d.c.}$ and on the fragility is much larger for the one-phase samples

($w_{P3OT} < 0.3$). Above $w_{P3OT} = 0.3$ the effect of composition on $\sigma_{d.c.}$ is much smaller than below $w_{P3OT} = 0.3$, especially at low temperatures.

Acknowledgements

This work was supported in part by DGES under grant PB96-0609, by CICYT under grant MAT96-0561, and by Fundación Ramón Areces. S. Moreno was supported by a FPI grant from MEC. G. Luengo was supported by MEC under a postdoctoral contract "Contrato de Reincorporación".

References

[1] Nakamura T. In: Nalwa HS, editor. Handbook of organic conductive molecules and polymers, vol. 1. New York: Wiley, 1997.
[2] Mott NF, Davis EA. Electronic processes in non-crystalline materials, Oxford: Clarendon Press, 1979.
[3] Ahlskog M, Reglon M, Heeger A-J. J Phys Condens Matter 1997;9:4145.
[4] Vatansever F, Hacaloglu J, Akbulut H, Toppare L. Polymer Intl 1996;41:237.
[5] De Paoli MA. In: Nalwa H-S, editor. Handbook of organic conductive molecules and polymers, vol. 2. New York: Wiley, 1997.
[6] Narkis M, Zilberman M, Siegmann A. Polymers for Advanced Technology 1997;8:525.
[7] Levon K, Margolina A, Patashinsky AZ. Macromolecules 1993;26:4061.
[8] Nielsen LE. Mechanical properties of polymers and composites, New York: Marcel Dekker, 1974.
[9] Levon K, Chu E, Ho K-S, Kwei TK, Mao J, Zheng WY, Laakso J. J Polym Sci B 1995;33:537.
[10] Kim MS, Levon K. J Polym Sci 1996;34:1665.
[11] Ngai KL, Rendell RW. In: Skotheim TA, editor. Handbook of conducting polymers, vol. 2. New York: Marcel Dekker, 1986.
[12] Chen SA, Liao Ch-S. Macromolecules 1993;26:2810.
[13] Díaz Calleja R. J Non-Crystalline Solids 1994;172–174:1413.
[14] Zetsche A, Fischer EW. Acta Polym 1994;45:168.
[15] MacDonald JR. Impedance spectroscopy-emphasizing solid materials and systems, New York: Wiley, 1987.
[16] Truong V-T, Ternan JG. Polymer 1995;36:905.
[17] Olmedo L, Hourquebie P, Jousse F. In: Nalwa HS, editor. Handbook of organic conductive molecules and polymers, vol. 3. New York: Wiley, 1997.
[18] Chen SA, Liao Ch-S. Synthetic Metals 1993;55–57:4936.
[19] Buerger DE, Boyd RH. Macromolecules 1989;22:2699.
[20] Holzer B, Strobl G. Acta Polymer 1996;47:40.
[21] Böttcher CJF, Bordewicjk P. 2nd. Theory of electric polarization, vol. 2. Amsterdam: Elsevier, 1978.
[22] Havriliak S, Havriliak SJ. Dielectric and mechanical relaxation in materials, Munich: Hanser, 1997.
[23] Alvarez F, Alegría A, Colmenero J. J Chem Phys 1991;44:7306.
[24] Ferry JD. Viscoelastic properties of polymers, 3rd edn. New York: Wiley, 1980.
[25] Moynihan CT. J Non-Crystalline Solids 1994;172–174:1395.
[26] Roland CM, Ngai KL. Macromolecules 1991;29:2261.
[27] Prolongo MG, Salom C, Masegosa RM, Moreno S, Rubio RG. Polymer 1997;38:5097.
[28] Tschoegl NW. The phenomenological theory of linear viscoelastic behaviour, Berlin: Springer, 1989.
[29] Provencher SW. Computer Phys Commun 1982;27:213.
[30] Weese J. Comput Phys Commun 1993;77:429.
[31] Alvarez F, Alegría A, Colmenero J. J Chem Phys 1995;103:798.
[32] Rizos AK, Fytas G, Semenov AN. J Chem Phys 1995;102:6931.
[33] Perrier G, Bergeret A. J Polym Sci B 1997;35:1349.
[34] MacDonald JR. J Non-Crystalline Solids 1997;210:70.